Absorption-aided x-ray emission tomography of planar targets

E. Stambulchik, E. Kroupp, Y. Maron, U. Zastrau, I. Uschmann, and G. G. Paulus

Absorption-aided x-ray emission tomography of planar targets

E. Stambulchik,[1] E. Kroupp,[1] Y. Maron,[1] U. Zastrau,[2] I. Uschmann,[2,3] and G. G. Paulus[2,3]

[1]*Faculty of Physics, Weizmann Institute of Science, Rehovot 76100, Israel*
[2]*Institute of Optics and Quantum Electronics, Friedrich-Schiller University, 07743 Jena, Germany*
[3]*Helmholtz Institute Jena, 07743 Jena, Germany*

Suggested is a tomography-like method for studying properties of solid-density plasmas with cylindrical symmetry, such as formed in the interaction of high-power lasers with planar targets. The method is based on simultaneous observation of the target x-ray fluorescence at different angles. It can be applied for validation of existing hypotheses and lately for reconstruction of the plasma properties with three-dimensional resolution. The latter becomes straightforward if the resonance x-ray self-absorption is negligible. The utility of the method is demonstrated by examples. © 2014 AIP Publishing LLC. [http://dx.doi.org/10.1063/1.4869246]

I. INTRODUCTION

Tomography is widely used in science, industry, and medicine. By taking two-dimensional images in multiple directions of a backlighted object, a three-dimensional reconstruction of the object's interior is possible.[1] Emission tomography (ET), instead of employing a backlighting source, is based on recording the emissivity of the object itself. For example, positron emission tomography (PET)[2] is widely used in medicine. Plasma, being a strong source of electromagnetic emission of different types, is a natural choice for ET employment.[3] If, in addition, the data are spectrally resolved, such diagnostics can provide a wealth of information, obtained by plasma spectroscopy techniques[4] for each point of the plasma volume. However, the use of 3D ET for plasma diagnostics has so far been restricted to rather long-living configurations, such as those found in magnetic-fusion devices and discharge arcs (e.g., Refs. 5–7). Evidently, highly transient plasmas, as formed, e.g., in pulsed-power devices or in laser-matter interactions, pose a practically insurmountable challenge to acquire a multitude of 2D images from different directions, during periods for which the plasma properties and shape do not change significantly. If, in addition, emission spectra are desired, the number of measurements required becomes larger, since one of the axes in the imaging plane is used for the spectral resolution, thus reducing the spatial dimensionality of a single scan to 1D. Short life times of transient plasmas also limit the signal intensity and, hence, the signal-to-noise ratio. Although the signal quality can be enhanced to some extent by using apertures with large acceptance angles and applying special post-processing algorithms,[8] this does not reduce the number of measurements required. These considerations, therefore, suggest that the application of ET to plasmas with axial symmetry, such as those formed in z-pinches[9] or in interactions of intense lasers with planar targets (assuming the incidence direction of the laser beam is close to the normal of the target surface), is more realistic. Below, we focus on studies of laser-matter interactions.

The interaction of short-duration ($\lesssim 1$ ps), high-intensity ($\gtrsim 10^{19}$ W/cm^2) laser pulses with solid targets is a highly complex issue. A suprathermal electron distribution is generated at the surface which subsequently penetrates the solid, distributing kinetic and electromagnetic field energy into the target. A large amount of energy deposited in a very short time to a small volume forms a unique state of the matter, often called Warm Dense Matter (WDM). The physics of WDM is an emerging and challenging field at the crossroad between physics of cold condensed matter and hot plasma physics. A thorough understanding of such strongly coupled plasmas[10] is of crucial importance for modeling astrophysical objects (e.g., cores of the giant planets[11]) and interaction of relativistic lasers with matter in inertial fusion research.[12] Furthermore, it is essential for progress in laser-driven x-ray sources,[13] which are suitable for backlighting in x-ray Thomson scattering experiments[14] and provide alternative radiation sources for a variety of scientific and medical applications.

X-ray emission spectroscopy is one of the most important diagnostic tools for studying WDM, since the visible and UV light cannot escape solid-density plasmas beyond a few angstroms of the skin depth. In a laser-produced plasma, the suprathermal electrons impact-ionize inner atomic shells, resulting in x-ray fluorescence, such as the characteristic $K\alpha$ spectral line. An x-ray spectrometer, using a doubly curved crystal positioned with its Rowland circle in the x–z plane, yields spectra that are spatially resolved in the y direction (projected onto the y' axis in the plane of the x-ray detector, such as a film or a CCD), see Fig. 1. Thus, in this respect, the doubly curved crystal functions as an ordinary cylindrical lens, integrating the radiation in the x–z plane. However, the entire radiation collected at each y is dispersed along the Rowland circle and projected onto the spectral axis (labeled as "Energy") of the x-ray detector.[15,16] Such a setup, by applying the inverse Abel transformation, allows for reconstructing the radial dependence of plasma properties.[17–19] However, the integration along the z axis (due to accumulation of photons emitted from different depths of the target) results in a weighted averaging of the spectra observed, precluding any depth-resolved conclusions to be made. In order to probe the z-dependence, multi-layered "sandwich" targets are used, with the relatively thin dopant layer placed at a

varying depth.[20] However, such specially manufactured targets are relatively expensive, and, more importantly, the multi-layered structure may introduce undesired effects due to the presence of materials with different mechanical, thermodynamic, and electromagnetic properties. In this study, we present an alternative, tomography-like method of resolving the z dimension that requires no specially prepared targets.

The proposed method utilizes absorption of the emitted radiation in the target. We note that the problem of absorption (also termed optical thickness or opacity) arises in the traditional ET methods if the object scanned is not optically thin. Then, the so called attenuation corrections need to be introduced in order to account for the absorption. Although numerical studies suggest that the emission field can be reconstructed with a reasonable accuracy even for optical thickness as high as 6–8,[21] the absorption is generally considered to be an obstacle. Contrary to that, in the present method, the absorption within a certain range of opacity is rather an aid.

II. METHOD

The measured spectrum $I_M(E, y; \theta)$ as a function of the photon energy E and coordinate y, observed at an angle θ to the target normal, is the local emissivity $I(E, r, z)$ integrated along both the x and z axes (see Fig. 1)

$$I_M(E, y; \theta) = \int_0^d dz \int_{-\infty}^\infty dx \, I(E, r, z) w(E, r, z; \theta). \quad (1)$$

Here, we assume that the detector is placed at a distance exceeding both the size of the radiating region (typically less than 1 mm) and the length of the crystal along the Rowland circle (typically, a few cm) at least by an order of magnitude. Hence, the entire object investigated is observed essentially
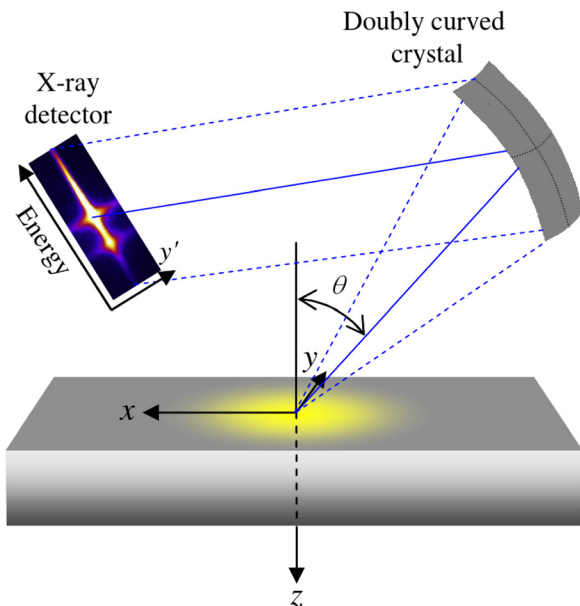
FIG. 1. Geometry of a typical experimental setup with planar targets. The target is irradiated by an intense laser beam (not shown) producing an x-ray-radiating hot spot, which is observed with an imaging spectrometer observing the target at the angle θ to the surface normal. The imaging axis is y. Darker colors towards the deeper target layers indicate a stronger photon attenuation.

at the same angle. d is the target thickness ($d = \infty$ for a bulk target), $r = (x^2 + y^2)^{1/2}$, and $w(E, r, z; \theta)$ is the attenuation factor due to the photon absorption in the target

$$w(E, r, z; \theta) = \exp\left[-\sec\theta \int_0^z dz' \kappa(E, r', z')\right], \quad (2)$$

where κ is the photon absorption coefficient, and r' satisfies the following system of equations:

$$\begin{cases} x'^2 + y^2 = r'^2 \\ x - x' = (z - z')\tan\theta \end{cases}, \quad (3)$$

describing a straight path from the point with coordinates (x, y, z) towards the observer. For $\pi/2 < \theta \leq \pi$, i.e., for observation from the rear side (evidently, inapplicable to bulk targets), the attenuation factor reads instead

$$w(E, r, z; \theta) = \exp\left[-|\sec\theta| \int_z^d dz' \kappa(E, r', z')\right]. \quad (4)$$

One can readily see that by varying the observation angle θ, photons emitted at different depths are attenuated differently. Indeed, while grazing observation angles ($\theta \approx \pi/2$) result in observing the emission that only comes from the outermost surface of the target, the closer to the normal the observation direction is, the larger the contributions from the deeper layers become. Therefore, observations made at different angles, together with the set of Eqs. (1)–(4), allow for testing specific hypotheses (e.g., results of analytic models or computer simulations). Evidently, such hypotheses should self-consistently also provide, in addition to the plasma spectral emissivity $I(E, r, z)$, the photon absorption coefficient $\kappa(E, r, z)$ at each point.

Alternatively, one may attempt to retrieve $I(E, r, z)$ from the spectra $I_M(E, y; \theta)$ for several values of θ. The principal difficulty here comes from the potential dependence of κ on the position (r, z) inside the target. In general, both resonant and non-resonant processes contribute to the absorption, such that $\kappa = \kappa_n + \kappa_r$, where subscripts "r" and "n" stand for the resonance and non-resonance absorption coefficients, respectively. We note that resonance absorption depends on the absorption spectrum and atomic level populations and, therefore, even under steady-state conditions is an intricate function of the electron energy distribution function, to which both thermal and suprathermal electrons contribute. Contrary to that, the non-resonance absorption can often be assumed to be independent of the position, i.e., $\kappa_n(E, r, z) = \kappa_0(E)$ in the target. This is justified when the target is largely homogeneous, which is the case in experiments with ps and sub-ps laser pulses, resulting in an x-ray emission on a ps-time scale;[22] such times are too short for the target to expand or compress noticeably. The calculations can be substantially simplified if, in addition, the resonance absorption is minor (for example, in a previous study,[27] the resonance absorption was inferred to yield a peak value on the order of 0.1 for the $K\alpha$ optical depth $\tau = \kappa_r d$, to be compared to the non-resonance one $\kappa_n d \approx 1.25$). Neglecting κ_r, Eqs. (2) and (4) become

$$w(z, E; \theta) = \begin{cases} \exp[-z\kappa_0(E)\sec\theta], & 0 \leq \theta < \pi/2 \\ \exp[-(z-d)\kappa_0(E)\sec\theta], & \pi/2 < \theta \leq \pi \end{cases}.$$

(5)

With these assumptions, we proceed by applying the inverse Abel transform to the measured spectrum:

$$\bar{I}(E, r; \theta) = \frac{1}{\pi} \int_r^\infty \frac{\partial I_M(E, y; \theta)}{\partial y} \frac{dy}{\sqrt{y^2 - r^2}}.$$

(6)

Using Eqs. (1) and (5) and swapping the integration order, one obtains

$$\bar{I}(E, r; \theta) = \int_0^d dz \, w(z, E; \theta) I(E, r, z),$$

(7)

which means that the Abel inversion recovers the radial dependence of the plasma emission. The spectrum thus inferred, however, is averaged with the proper weight $w(z, E; \theta)$ over the target depth d. Let us introduce

$$\xi = \kappa_0(E)\sec\theta.$$

(8)

Then, Eqs. (5) and (7) can be rewritten as

$$w(z, E; \xi) = \begin{cases} e^{-z\xi}, & \xi > 0 \\ e^{-(z-d)\xi}, & \xi < 0 \end{cases}$$

(9)

and

$$\bar{I}(E, r; \xi) = \int_0^d dz \, w(z, E; \xi) I(E, r, z),$$

(10)

respectively. Without loss of generality, we can drop the E and r dependencies (they can be reintroduced at any stage). Therefore, we need to restore $f(z)$ given that $F(\xi)$

$$F(\xi) = \int_0^d dz f(z) e^{-z\xi} \times \begin{cases} 1, & \xi > 0 \\ e^{-d|\xi|}, & \xi < 0 \end{cases}$$

(11)

is known. Provided the data are of sufficient quality (i.e., with high signal-to-noise ratio) and extent (i.e., available for many angles), one can in principle invert Eq. (11) numerically. For example, with measurements performed at N different angles, and assuming that the target consists of N layers each of thickness d/N, Eq. (11) is transformed to a system of N linear equations (we remind the reader that this is done independently at each E and r).

Evidently, this method is applicable for targets with a thickness comparable to the non-resonance photon pathlength κ_n^{-1} in the target. For example, the non-resonance photon pathlength of a solid-state titanium is practically constant around the $K\alpha$-line energy and equals to $\approx 20\,\mu m$.[23] Thus, 5–20-μm-thick foils can be used for such tomography-like measurements. If the measurements are performed from both the front and rear sides of the target, the usable thickness is doubled.

A slight axial asymmetry, resulting, e.g., from the laser beam incident at some angle to the target normal, can be accounted for by applying, instead of Eq. (6), a modified Abel inversion procedure.[24–26]

III. EXAMPLE

We now demonstrate the usefulness of the method. Let us assume the simplest type of measurements that integrate over the entire foil target (without spatial resolution in the y direction) and a moderate spectral resolution that is only sufficient to distinguish $K\alpha$ radiation from the x-ray background. Thus, measured is the total $K\alpha$ radiance as a function of the observation angle. Furthermore, for the sake of simplicity, the resonance absorption is assumed to be negligible, as discussed above. The target, made of a material with $\kappa_n^{-1} = 20\,\mu m$, has a thickness of 25 μm. We now consider a series of models where the $K\alpha$ yield in the target decreases with the depth as $\sim \exp(-z/l)$. This is shown in Fig. 2(a) for $l = \infty$, 20, 10, and 5 μm. The respective radiances as a function of the observation angle, normalized to that at the frontal observation, are shown in Fig. 2(b). As is clearly seen, the
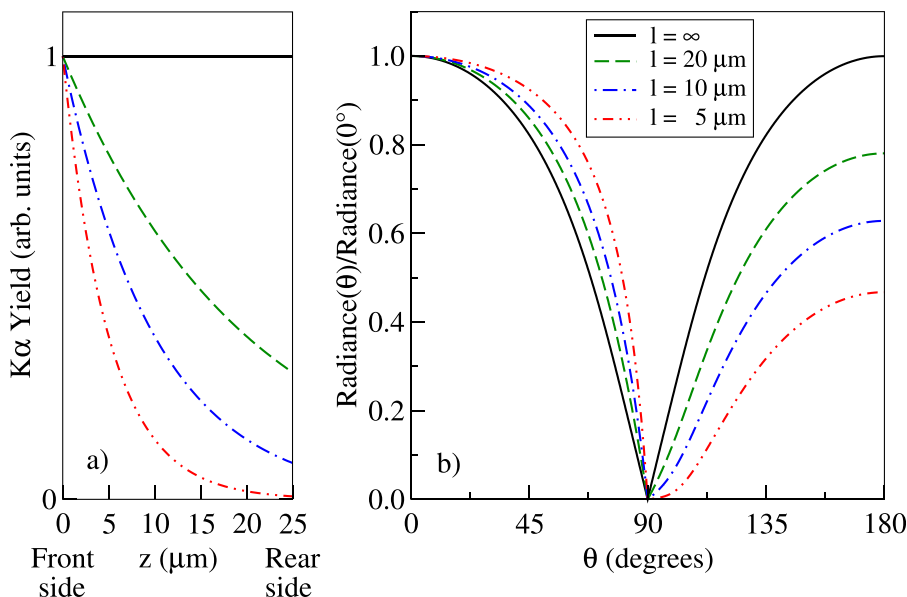
FIG. 2. Demonstration of the method: (a) A few models of $K\alpha$-yield z-dependence in a 25-μm-thick foil made of a material with a photon free path length of 20 μm; (b) Relative (to the zero-degree direction of observation) intensity of the observed radiation as a function of the polar angle θ.

angular dependencies differ significantly, allowing for discriminating between these simple models using as few as two measurements. Indeed, the ratio of the radiances measured at observation angles close to the rear- and front-side normals varies from unity (homogeneous $K\alpha$ yield, $l = \infty$) to more than two for $l = 5\,\mu$m. Alternatively, with the "reference" directions chosen to be $60°$ to the front and rear normals, the ratio varies more than *fourfold*. We note that since only the relative variations of the radiation intensity are used, no absolute calibration of the data acquisition system is required, thus simplifying the experimental setup and reducing instrumental uncertainties.

Evidently, performing measurements at only two directions is not sufficient for inferring z distributions that are described by models more complex than the simple one-parameter distribution assumed in this example. In general, the number of observations (at different angles) should exceed the number of parameters in the theoretical model to be tested.

IV. CONCLUSIONS

We suggested an absorption-aided x-ray emission tomography method for studying properties of high-density radiating matter with cylindrical symmetry and significant extent in the radial direction, e.g., such as formed in interactions of high-power lasers with foil targets. The method utilizes simultaneous observations of the planar target at a few different angles and allows for reconstruction of the plasma properties with radial and axial spatial resolutions. No specially manufactured (e.g., multi-layered) targets are required.

ACKNOWLEDGMENTS

[1]G. T. Herman, *Fundamentals of Computerized Tomography: Image Reconstruction from Projections*, 2nd ed. (Springer, New York, 2009).
[2]*Positron Emission Tomography*, edited by D. L. Bailey, D. W. Townsend, P. E. Valk, and M. N. Maisey (Springer-Verlag London Limited, New York, 2005).
[3]V. V. Pickalov and T. S. Mel'nikova, *Tomography of Plasma* (Nauka, Novosibirsk, 1995).
[4]H. R. Griem, *Principles of Plasma Spectroscopy* (Cambridge University Press, Cambridge, UK, 1997).
[5]M. Hino, T. Aono, M. Nakajima, and S. Yuta, Appl. Opt. **26**, 4742 (1987).
[6]L. A. Shmaenok, S. V. Golovkin, V. N. Govorun, A. V. Ekimov, N. N. Salashchenko, V. V. Pickalov, V. P. Belik, F. C. Schüller, A. J. H. Donné, A. A. M. Oomens, K. A. Prokhorov, S. S. Andreev, A. A. Sorokin, B. G. Podlaskin, and L. V. Khasanov, Rev. Sci. Instrum. **72**, 1411 (2001).
[7]X. Franceries, P. Freton, J.-J. Gonzalez, F. Lago, and M. Masquère, J. Phys. D: Appl. Phys. **38**, 3870 (2005).
[8]S. V. Shabanov and I. B. Gornushkin, Spectrochim. Acta, Part B **66**, 413 (2011); S. Shabanov and I. Gornushkin, J. Quant. Spectrosc. Radiat. Transfer **113**, 518 (2012).
[9]D. D. Ryutov, M. S. Derzon, and M. K. Matzen, Rev. Mod. Phys. **72**, 167 (2000).
[10]R. Redmer and G. Röpke, Contrib. Plasma Phys. **50**, 970 (2010).
[11]T. Guillot, Science **286**, 72 (1999).
[12]M. Tabak, J. Hammer, M. Glinsky, W. Kruer, S. Wilks, J. Woodworth, E. Campbell, M. Perry, and R. Mason, Phys. Plasmas **1**, 1626 (1994).
[13]C. Reich, P. Gibbon, I. Uschmann, and E. Förster, Phys. Rev. Lett. **84**, 4846 (2000).
[14]S. Glenzer and R. Redmer, Rev. Mod. Phys. **81**, 1625 (2009).
[15]T. Missalla, I. Uschmann, E. Förster, G. Jenke, and D. von der Linde, Rev. Sci. Instrum. **70**, 1288 (1999).
[16]I. Uschmann, P. Gibbon, D. Klöpfel, T. Feurer, E. Förster, P. Audebert, J.-P.Geindre, J.-C. Gauthier, A. Rousse, and C. Rischel, Laser Part. Beams **17**, 671 (1999).
[17]U. Zastrau, P. Audebert, V. Bernshtam, E. Brambrink, T. Kämpfer, E. Kroupp, R. Loetzsch, Y. Maron, Y. Ralchenko, H. Reinholz, G. Röpke, A. Sengebusch, E. Stambulchik, I. Uschmann, L. Weingarten, and E. Förster, Phys. Rev. E **81**, 026406 (2010).
[18]U. Zastrau, A. Sengebusch, P. Audebert, E. Brambrink, R. Faüstlin, T. Kämpfer, E. Kroupp, R. Loetzsch, Y. Maron, H. Reinholz, G. Röpke, E. Stambulchik, I. Uschmann, and E. Förster, High Energy Density Phys. **7**, 47 (2011).
[19]G. Cristoforetti, M. P. Anania, A. Y. Faenov, A. Giulietti, D. Giulietti, S. B. Hansen, P. Koester, L. Labate, T. Levato, T. A. Pikuz, and L. A. Gizzi, Phys. Rev. E **87**, 023103 (2013).
[20]K. B. Wharton, S. P. Hatchett, S. C. Wilks, M. H. Key, J. D. Moody, V. Yanovsky, A. A. Offenberger, B. A. Hammel, M. D. Perry, and C. Joshi, Phys. Rev. Lett. **81**, 822 (1998).
[21]A. Likhachev and V. Pikalov, Opt. Spectrosc. **88**, 667 (2000).
[22]P. M. Nilson, J. R. Davies, W. Theobald, P. A. Jaanimagi, C. Mileham, R. K. Jungquist, C. Stoeckl, I. A. Begishev, A. A. Solodov, J. F. Myatt, J. D. Zuegel, T. C. Sangster, R. Betti, and D. D. Meyerhofer, Phys. Rev. Lett. **108**, 085002 (2012).
[23]B. L. Henke, E. M. Gullikson, and J. C. Davis, At. Data Nucl. Data Tables **54**, 181 (1993).
[24]Y. Yasutomo, K. Miyata, S. I. Himeno, T. Enoto, and Y. Ozawa, IEEE Trans. Plasma Sci. **9**, 18 (1981).
[25]P. Tomassini and A. Giulietti, Opt. Commun. **199**, 143 (2001).
[26]G. Cristoforetti, S. Legnaioli, V. Palleschi, A. Salvetti, E. Tognoni, and P. Tomassini, Spectrochim. Acta, Part B **60**, 888 (2005).
[27]E. Stambulchik, V. Bernshtam, L. Weingarten, E. Kroupp, D. Fisher, Y. Maron, U. Zastrau, I. Uschmann, F. Zamponi, E. Förster, A. Sengebusch, H. Reinholz, G. Röpke, and Y. Ralchenko, J. Phys. A: Math. Theor. **42**, 214056 (2009).